Enhanced catalytic performance for metathesis reactions over ordered tungsten and aluminum co-doped mesoporous KIT-6 catalysts†

Huan Liu,[ab] Kai Tao,*[a] Peipei Zhang,[a] Wei Xu[a] and Shenghu Zhou*[a]

Ordered tungsten and aluminum co-doped mesoporous KIT-6 catalysts (W-Al-KIT-6) with different Si/Al molar ratios were successfully synthesized by a one-pot synthesis method. The obtained W-Al-KIT-6 catalysts were tested for catalytic conversion of 1-butene and ethene to propene *via* isomerization of 1-butene to 2-butene and subsequent cross metathesis of 2-butene and ethene. Various characterization techniques, such as ICP-OES, XRD, BET, TEM, Raman, XPS and NH_3-TPD, were used to characterize the catalysts. The introduction of Al did not change the mesoporous structure of KIT-6 when the nominal Si/Al was 10, 20 or 30. Moreover, the sample demonstrated a larger amount of acidic sites. The W-Al-KIT-6 catalysts with suitable Si/Al ratios illustrated a superior catalytic performance to W-KIT-6 catalyst. The origin of catalytic performance enhancement over W-Al-KIT-6 catalysts is preliminarily discussed and ascribed to the highly disperse W species and a large amount of acidic sites. The acidic sites were formed by the introduction of a suitable amount of Al in the W-KIT-6 framework, which accelerated the isomerization of 1-butene to 2-butene and promoted the cross metathesis of 2-butene and ethene to propene.

1. Introduction

With the increasing demand for propene, cross-metathesis of butene and ethene to propene has attracted more and more attention in recent years.[1] Supported WO_3 catalysts, showing moderate activity, outstanding stability, anti-poisoning property, as well as low price, are highly desirable for industrial metathesis.[2,3]

The catalytic performance of supported tungsten oxides for olefin metathesis is determined by many factors. The supports have a significant influence on the physico-chemical properties of the catalyst, such as structure and dispersion of tungsten oxide species, and thus significantly influence the catalytic performance.[4] Conventional support materials for metathesis catalysts include commercially available silica gel, γ-Al_2O_3, α-Al_2O_3, and mixed oxides such as SiO_2–Al_2O_3[5] and zeolite–Al_2O_3.[6] Compared with these traditional supports, mesoporous materials show uniform pores, large BET surface areas and pore volumes, which are beneficial for the dispersion of active species and providing rapid transportation channels for reactants and products. Thus, great efforts have been made to develop highly efficient mesoporous catalysts for various reactions[7,8] over the last decades. To date, many mesoporous materials have been explored in olefin metathesis[9] such as HMS,[10] SBA-15,[11,12] MCM-41,[13] and FDU-12.[14] In general, mesoporous catalysts showed much higher catalytic activity than conventional SiO_2 or Al_2O_3 supported catalysts, due to the highly dispersed active species on the mesoporous supports.

On the other hand, it has been demonstrated that the Brønsted acidity of the supports would be beneficial for olefin metathesis.[6] Literature has revealed that alumina supported tungsten oxides exhibit strong acid sites and tungsten-support interaction, but very strong acid sites could induce by-reactions such as cracking and isomerization.[15] In contrast, silica supported tungsten oxides were barely acidic and could suppress the by-reactions.[16] However, the weak interaction between W species and silica could result in poor dispersion of tungsten oxide species, causing poor catalytic performance. Mixed silica–alumina materials with moderate acidity and interaction between metal and support are promising as catalyst supports for olefin metathesis reactions. Xu *et al.*[6] reported that WO_3/HY–Al_2O_3 catalysts exhibited higher activity than WO_3/Al_2O_3 with HY content in the range of 0–30 wt%. The improved catalytic performance over WO_3/HY–Al_2O_3 was ascribed to the moderate acidity of the supports and the suitable interaction between W species and support. The same phenomenon was also found in supported Mo or Re catalysts. It has been reported in the literature that MoO_3/Al_2O_3–SiO_2 and Re_2O_7/Al_2O_3–SiO_2 catalysts were more active

[a] *Ningbo Institute of Materials Technology and Engineering, Chinese Academy of Sciences, Ningbo, Zhejiang 315201, China. E-mail: zhoush@nimte.ac.cn, taokai@nimte.ac.cn; Fax: +86 574 86685043; Tel: +86 574 86696927*

[b] *Shanghai Key Laboratory of Atmospheric Particle Pollution and Prevention (LAP3), Department of Environmental Science and Engineering, Fudan University, Shanghai 200433, China*

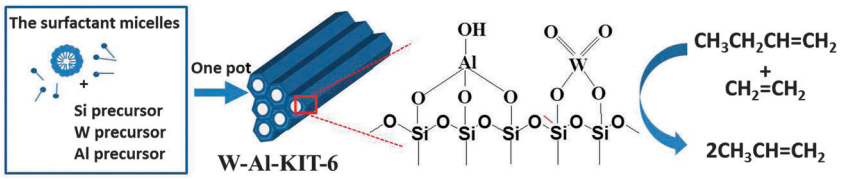

Scheme 1 The schematic of the synthesis of ordered tungsten and aluminum co-doped mesoporous KIT-6 materials.

than alumina or silica supported catalysts due to high dispersion of active species and moderate acidity.[17–19]

Herein, we first report a one-pot synthesis of ordered tungsten and aluminum co-doped mesoporous KIT-6 materials (W-Al-KIT-6) for the metathesis of 1-butene and ethene to propene. KIT-6, a mesoporous silica with 3D interconnected large mesopores, has been shown to be an advanced support for many reactions.[20,21] In our previous study, we successfully synthesized tungsten doped KIT-6 catalysts (W-KIT-6), and the obtained W-KIT-6 exhibited excellent catalytic performance for metathesis reactions.[22,23] In this study, Al and W were co-doped into the KIT-6 framework simultaneously by a one-pot method. The schematic of the synthesis of tungsten and aluminum co-doped W-Al-KIT-6 is shown in Scheme 1. Al is introduced to form the acid center and improve the performance of the catalysts. The influence of Si/Al ratio on physico-chemical properties was systematically investigated with various characterization techniques, and the catalytic performance for metathesis of 1-butene and ethene to propene over W-Al-KIT-6 with different Si/Al ratios was also studied.

2. Experimental section

2.1. Chemicals

Poly(ethylene glycol)-*block*-poly(propylene glycol)-*block*-poly(ethylene glycol) (P123, M_w = 5800, EO20PO70EO20) was purchased from Aldrich as the structure directing agents. Tetraethyl orthosilicate (TEOS, AR) as the silica source was purchased from Aladdin. Sodium tungstate dihydrate ($Na_2WO_4{\cdot}2H_2O$, AR), hydrochloric acid (HCl, AR), and *n*-butanol (AR) were purchased from Sinopharm Chemical Reagent Co., Ltd. Aluminum-isopropoxide as the Al source was purchased from Chengdu Gray West Chemistry Technology Company. Ammonium metatungstate ($(NH_4)_6H_2W_{12}O_{40}{\cdot}xH_2O$) was obtained from Kunshan Xingbang W&M Technology Company. All chemicals were used as received without further purification.

2.2. Catalyst preparation

2.2.1 Synthesis of W-KIT-6. W-KIT-6 catalysts with a Si/W ratio of 40/1 was prepared according to our previous study.[22] Typically, 3.0 g of P123 was dissolved in 108.5 g of deionized water, and 3.0 g of 1-butanol and 5.9 g of HCl (35 wt%) were added to the abovementioned solution. The mixture was vigorously stirred at 35 °C for 1 h and then 6.45 g of TEOS was slowly added into the solution. After that, the mixture was vigorously stirred at 35 °C for 1 h, and 0.25 g of sodium tungstate dissolved in 6 mL of water (Si/W = 40/1) was added dropwise into the abovementioned solution. The obtained mixture was further stirred for another 24 h. The resultant mixture was transferred to a Teflon-lined autoclave and heated at 100 °C for 24 h. The solid products were collected by filtering, washing thoroughly with deionized water and drying at 100 °C overnight. Finally, the powders were calcined in a muffle furnace at 550 °C for 4 h at a heating rate of 1.0 °C min^{-1} to remove P123 surfactants. KIT-6 was also synthesized using the same procedure as that of W-KIT-6 without adding sodium tungstate.

2.2.2 One-pot synthesis of W-Al-KIT-6. The incorporation of Al in W-KIT-6 was carried out by a one-pot synthesis method using aluminum-isopropoxide as the Al source. In a typical synthesis for W-Al-KIT-6 with a Si/Al ratio of 10/1, 0.63 g of aluminum-isopropoxide was dissolved in a solution containing 108.5 g of deionized water and 5.9 g of HCl (35 wt%). The solution was vigorously stirred at 35 °C for at least 1 h, and then 3.0 g of P123 and 3.0 g of 1-butanol were added into the abovementioned solution. The mixture was vigorously stirred at 35 °C for 1 h, and then 6.45 g of TEOS (Si/Al = 10/1) was slowly added into the solution. Furthermore, the mixture was vigorously stirred at 35 °C for 1 h. A solution containing 0.25 g of sodium tungstate dihydrate and 6 mL of water (Si/W = 40) was added dropwise into the abovementioned solution, and the resultant mixture was stirred for another 24 h. W-Al-KIT-6 was obtained after the same hydrothermal treatment, collecting procedures and calcination process as those of W-KIT-6. W-Al-KIT-6 with different Si/Al ratios were synthesized using the same procedures, except that the amount of aluminum-isopropoxide was changed according to the desired nominal Si/Al ratios. The W-Al-KIT-6 materials with Si/Al ratios of 1/1, 10/1, 20/1 and 30/1 were denoted as W-Al-KIT-6-1, W-Al-KIT-6-10, W-Al-KIT-6-20 and W-Al-KIT-6-30, respectively.

2.2.3 Preparation of control WO_3/SiO_2 catalyst. A control WO_3/SiO_2 catalyst was prepared by impregnating commercial silica gel (BET surface area: 399.0 m^2 g^{-1}, Qingdao Haiyang Chemical Co. Ltd) with an aqueous solution of ammonium metatungstate. The impregnated sample was dried at 100 °C overnight and subjected to an identical calcination procedure to W-KIT-6 catalyst. The loading of W was identical to that of W-KIT-6.

2.3. Catalyst characterization

Elemental analysis was conducted by inductively coupled plasma-optical emission spectroscopy (ICP-OES) using a Perkin-Elmer OPTIMA 2100 DV optical emission spectrometer. Brunauer–Emmett–Teller (BET) surface area, pore volume, and pore size was obtained using a Micromeritics ASAP 2020M adsorption apparatus. Prior to measurement, the sample was degassed under vacuum at 200 °C for 3 h. Small angle and wide angle

X-ray diffraction patterns (XRD) were recorded on a Bruker D8 Advance X-ray diffractometer using Cu Kα radiation. Raman spectra were obtained using a Renishaw Raman spectrometer equipped with a microscope (laser wavelength of 532 nm). Transmission electron microscopy (TEM) image was obtained on a JEOL 2100 transmission electron microscope operated at 200 kV. The sample was dispersed in ethanol by sonication and dropped onto a carbon-coated copper grid followed by natural evaporation. X-ray photoelectron spectroscopy (XPS) experiments were performed on an AXIS ULTRA DLD multifunctional X-ray photoelectron spectroscopy with an Al source. Temperature-programmed desorption of ammonia (NH_3-TPD) was carried out in a quartz micro-reactor. The as-prepared sample (50.0 mg) was pretreated in N_2 at 600 °C for 0.5 h prior to NH_3-TPD measurement, and then a stream of 10/90 (v/v) NH_3/N_2 was introduced for adsorption at room temperature for 0.5 h. The sample was further purged by N_2 for 2 h in order to remove the physically absorbed NH_3. Temperature-programmed desorption of ammonia was carried out from 50 °C to 800 °C with a ramping rate of 10 °C min^{-1}, and the amount of desorbed NH_3 was monitored by a thermal conductivity detector (TCD).

2.4. Catalytic conversion of 1-butene and ethene to propene

Catalytic conversion of 1-butene and ethene to propene was carried out in a fixed-bed stainless steel micro-reactor (i.d. 10 mm). In each run, 1.0 g of catalyst (20–40 mesh) was placed at the center of the reactor, and the catalyst layer was below and above supported by an inert SiO_2 bead layer. The catalysts were pretreated by pure N_2 at 550 °C for 4 hours (0.1 MPa, 30 mL min^{-1}). After cooling to the reaction temperatures, C_2H_4 and 1-C_4H_8 (98%, Dalian special gas company) were directly delivered to the reactor from cylinders. The gas flow rates of C_2H_4 and 1-C_4H_8 were controlled by two mass flow controllers (MFC) to maintain the molar ratio of C_2H_4/1-C_4H_8 equal to 2/1. The metathesis reactions were carried out at ambient pressure, reaction temperature from 400 to 500 °C, and gas hourly space velocity (WHSV) of 0.8 h^{-1}. All products were analyzed online using a gas chromatograph equipped with a flame ionization detector (FID). 1-Butene conversion and product selectivity were calculated using the following formulas:

$$x_{1\text{-butene}} = \frac{[C_3^=]_n + 2[2-C_4^=]_n}{[C_3^=]_n + 2[1-C_4^=]_n + 2[2-C_4^=]_n + 2[\text{iso-}C_4^=]_n} \quad (1)$$

$$s_{\text{propene}} = \frac{[C_3^=]_m}{[C_3^=]_m + [2-C_4^=]_m + [\text{iso-}C_4^=]_m} \quad (2)$$

$$s_{2\text{-butene}} = \frac{[2-C_4^=]_m}{[C_3^=]_m + [2-C_4^=]_m + [\text{iso-}C_4^=]_m} \quad (3)$$

where $[C_3^=]_n$, $[1\text{-}C_4^=]_n$, $[2\text{-}C_4^=]_n$ and $[\text{iso-}C_4^=]_n$ are the molar fractions of each component in the effluent gas, and $[C_3^=]_m$, $[1\text{-}C_4^=]_m$, and $[\text{iso-}C_4^=]_m$ are the mass fractions of each component in the effluent gas.

3. Results and discussion

3.1. Characterization of catalysts

3.1.1 Elemental analysis. ICP-OES analysis was performed to determine the real content of Na, W and Al in the final products. The result suggested that only trace amounts of Na (below 0.1 wt%) remained in the catalyst, since the sample was washed thoroughly before calcination. Table 1 summarizes the real loading of W and Al in the final catalysts. Approximately 67–80% of W species in the initial synthesis gel was introduced in the final W-Al-KIT-6, and this tendency was consistent with the literature.[22] In contrast, approximately 21% of Al species in the initial synthesis gel was introduced in the final W-Al-KIT-6 at Si/Al ratios ranging from 10/1 to 30/1, whereas ~40% of Al species in the initial synthesis gel was introduced in the final products at the Si/Al ratio of 1/1. A limited amount of Al doped in the final product was also reported in the literature.[24,25] In the acidic medium, most of Al species were in cationic rather than oxo forms (necessary for formation of Si–O–Al linkages), restricting the amount of Al species in the final products.

3.1.2 Transmission electron microscopy. TEM images of various samples are illustrated in Fig. 1. As shown in Fig. 1a, KIT-6 exhibits a three dimensional (3D) ordered mesoporous structure, which is consistent with the literature.[26,27] The W doped KIT-6 samples (W-KIT-6) in Fig. 1b also show a well-ordered mesoporous structure, except for a few irregular domains at the peripheries of the materials. The introduction of Al did not change the structure/texture/appearance of the sample (when Si/Al in 10, 20 or 30), as shown in Fig. 1c–e. However, for the W-Al-KIT-6-1 (Fig. 1f) at the highest ratio of Al/Si, the ordered mesoporous structures disappeared, showing disordered structures. It is suggested that the introduction of a proper amount of Al is beneficial for maintenance of mesoporous structures and excess Al introduction causes the collapse of the mesoporous structure.

3.1.3 Nitrogen physisorption. The N_2 adsorption isotherms and BJH pore size distributions of KIT-6, W-KIT-6 and W-Al-KIT-6 materials are shown in Fig. 2. Except for W-Al-KIT-6-1, all samples showed type IV isotherms with H1 hysteresis loops, which revealed that all samples had ordered mesoporous channels.[28] The sharp capillary condensation feature at relative pressure of 0.6–0.8 (P/P_0) indicates the existence of uniform pores in all the samples. It can be clearly observed that all samples, except W-Al-KIT-6-1, show narrow pore-size distributions. An increase of the Si/Al ratio typically resulted in a small

Table 1 Elemental analysis of various catalysts by ICP-OES

	Si/W (molar)		Si/Al (molar)		Product	
Catalysts	Gel	Product	Gel	Product	W (wt%)	Al (wt%)
KIT-6	N/A	N/A	N/A	N/A	N/A	N/A
WO_3/SiO_2	40/1	N/A	N/A	N/A	4.85	N/A
W-KIT-6	40/1	58/1	N/A	N/A	5.01	N/A
W-Al-KIT-6-30	40/1	55/1	30/1	138/1	5.26	0.30
W-Al-KIT-6-20	40/1	51/1	20/1	94/1	5.51	0.44
W-Al-KIT-6-10	40/1	53/1	10/1	47/1	5.06	0.88
W-Al-KIT-6-1	40/1	59/1	1/1	2.5/1	3.49	12.93

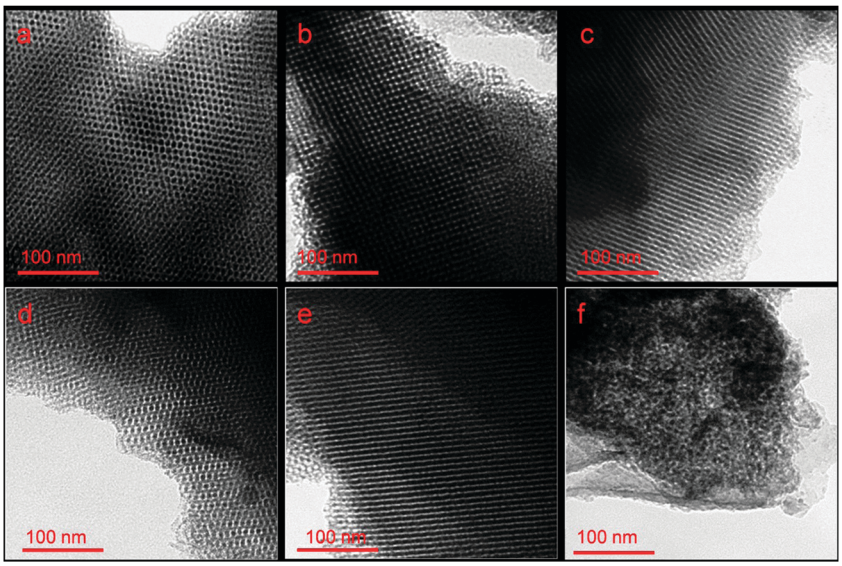

Fig. 1 TEM images showing (a) KIT-6; (b) W-KIT-6; (c) W-Al-KIT-6-30; (d) W-Al-KIT-6-20; (e) W-Al-KIT-6-10; and (f) W-Al-KIT-6-1. Scale bars are 100 nm.

increase in the average pore size; therefore, the pore diameter showed a slight shift. For W-Al-KIT-6-1, the isotherm and pore size distribution was significantly different from that of W-KIT-6 and W-Al-KIT-6 catalysts with Si/Al of 10, 20 or 30. It has been indicated that the ordered mesoporous structure of KIT-6 disappeared as confirmed by the TEM observation (Fig. 1f).

Table 2 summarizes the BET surface areas, pore volumes and mean pore sizes of different samples. The reduction of BET surface areas and pore volumes are observed for W-KIT-6, as compared with those of KIT-6. However, the introduction of an appropriate amount of Al, W-Al-KIT-6-30, W-Al-KIT-6-20 or W-Al-KIT-6-10 showed slightly improved BET surface area, pore volume and pore size as compared with that of W-KIT-6. This suggested that the incorporation of a suitable amount of Al did not disturb the mesoporous structure. In contrast, the W-Al-KIT-6-1 sample with the highest Al/Si ratio exhibited a drastic reduction of BET surface areas due to the collapse of the mesoporous structures and blocking of pores caused by excess aluminum.

Table 2 BET surface areas, pore volumes, and pore sizes of various catalysts

Catalysts	a_0[a] (nm)	BET surface area ($m^2\ g^{-1}$)	Pore volume ($cm^3\ g^{-1}$)	Average pore size (nm)	Acidity amount ($\mu mol\ g^{-1}$)
KIT-6	19.6	835	0.98	4.6	68.1
W-KIT-6	21.0	721	0.81	4.6	126.3
W-Al-KIT-6-30	20.6	764	0.93	5.1	191.6
W-Al-KIT-6-20	20.6	758	0.94	5.1	207.6
W-Al-KIT-6-10	20.8	754	1.1	6.2	232.8
W-Al-KIT-6-1	N/A	265	1.0	15.7	274.6

[a] Unit cell parameter calculated from the formula $a_0 = 6^{1/2}d_{211}$.

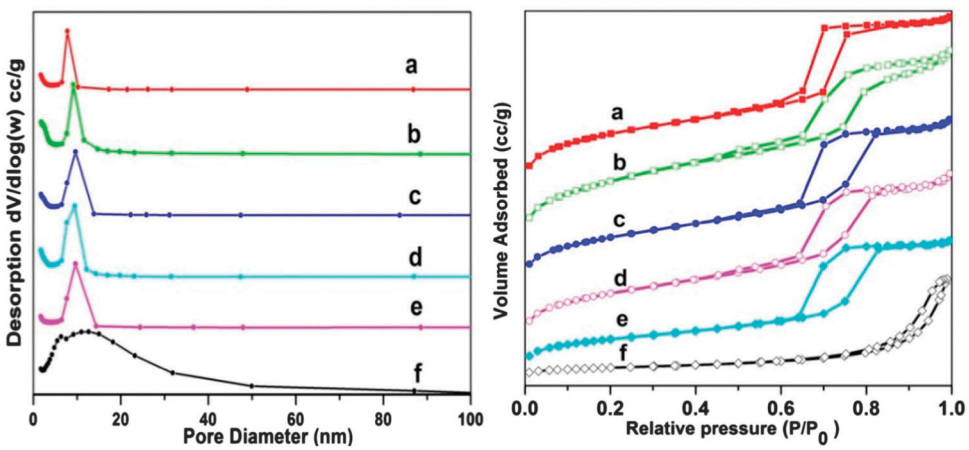

Fig. 2 N_2 adsorption–desorption isotherms (left panel) and pore size distributions (right panel) showing (a), KIT-6; (b) W-KIT-6; (c) W-Al-KIT-6-30; (d) W-Al-KIT-6-20; (e) W-Al-KIT-6-10 and (f) W-Al-KIT-6-1.

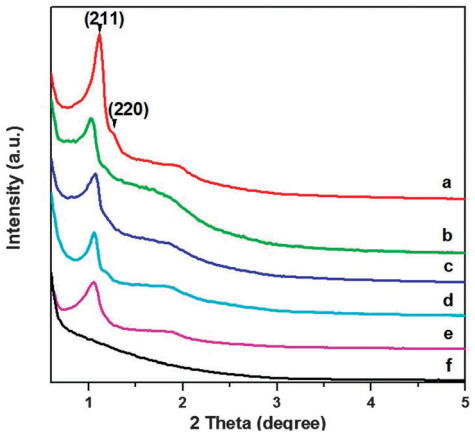

Fig. 3 Small-angle XRD patterns of various samples showing (a) KIT-6; (b) W-KIT-6; (c) W-Al-KIT-6-30; (d) W-Al-KIT-6-20; (e) W-Al-KIT-6-10; and (f) W-Al-KIT-6-1.

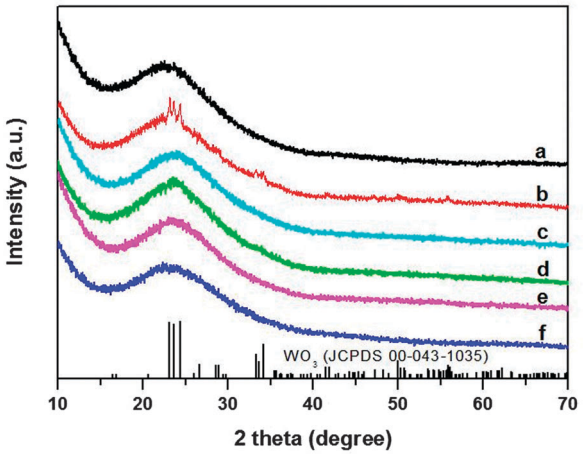

Fig. 4 Wide-angle XRD patterns of various samples showing (a) KIT-6; (b) W-KIT-6; (c) W-Al-KIT-6-30; (d) W-Al-KIT-6-20; (e) W-Al-KIT-6-10; and (f) W-Al-KIT-6-1. Vertical lines indicate the diffractions of crystalline WO_3 (JCPDS 00-043-1035).

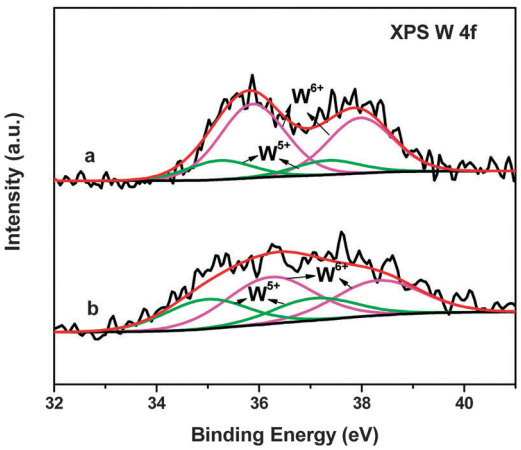

Fig. 5 XPS spectra showing (a) W-KIT-6; and (b) W-Al-KIT-6-10.

3.1.4 X-ray diffraction. Small angle XRD measurement was used to study the mesoporosity of various samples, and the results are presented in Fig. 3. A well-resolved diffraction peak in the 1.0°–1.1° range was observed for KIT-6, which could be indexed as the (211) reflection in the bicontinuous cubic *Ia3d* symmetry reported for KIT-6.[29] Moreover, the existence of a broad shoulder corresponding to (220) reflection further indicated ordered mesoporous structures. Except for the W-Al-KIT-6-1 sample at the highest ratio of Al/Si (Fig. 3f), all samples exhibited the well resolved diffraction patterns similar to KIT-6, confirming that the ordered mesoporous structure of KIT-6 was maintained after the incorporation of W and Al with suitable Si/Al ratios (10/1, 20/1 or 30/1). For W-Al-KIT-6-1, the absence of diffraction peaks in small angles suggested the collapse of mesoporous structures. In addition, cubic unit cell parameters (a_0) of samples are also calculated and presented in Table 2. It was found that the unit cell parameter a_0 increased after introducing W and Al atoms in the framework of KIT-6, accompanied by the shift of (211) reflections to lower angles in Fig. 3. This phenomenon may be caused by doping tungsten with larger atomic radius compared to that of Si^{4+}.[30,31]

Wide-angle XRD profiles of various samples are shown in Fig. 4. KIT-6 showed a broad peak in the 2θ range from 15° to 30°, which are the characteristic diffractions of amorphous silica. Obvious crystalline WO_3 diffractions (JCPDS 00-043-1035) are observed for W-KIT-6 in Fig. 4b, which is due to the formation of WO_3 extra-framework at a high W loading.[22] In contrast, no WO_3 diffractions are observed for all W-Al-KIT-6 samples (Fig. 4c–f), indicating that the W species are highly dispersed in W-Al-KIT-6 samples. It is concluded that the introduction of Al in W-KIT-6 by the current one-pot synthesis method could enhance the dispersion of W species, which may further enhance the catalytic performance for metathesis of 1-butene and ethene to propene.

3.1.5 X-ray photoelectron spectroscopy. XPS experiments were carried out to investigate the effect of Al doping on the oxidation states of tungsten. Fig. 5 shows the XPS spectra of the W-KIT-6 and W-Al-KIT-6-10 samples. The XPS curves were fitted according to the theory of Doniach and Sunjic.[32] The binding energies of 35.9–36.2 eV and 38.0–38.3 eV were attributed to $4f_{7/2}$ and $4f_{5/2}$ of W^{6+} species, whereas the binding energies of 37.0–37.3 and 34.9–35.2 eV were assigned to $4f_{5/2}$ and $4f_{7/2}$ of W^{5+} species, respectively.[33–35] The presence of W^{5+} species in W-KIT-6 sample was consistent with our previous study.[22] W^{5+} species was also observed in the W-Al-KIT-6 sample. Table S1 (ESI†) summarizes the molar percentage of W^{6+} and W^{5+} species in W-KIT-6 and W-Al-KIT-6-10 samples. The molar percentage of W^{5+} species in W-KIT-6 was 20.6%, whereas the molar percentage of W^{5+} in W-Al-KIT-6-10 samples increased to 37.5%. The presence of a high concentration of W^{5+} species could favor olefin metathesis, as suggested by previous studies.[6,22]

3.1.6 NH_3-temperature programmed desorption. NH_3-TPD technique was used to study the effect of aluminum doping on the acidity of catalysts, and the results are shown in Fig. 6. KIT-6 showed a weak desorption peak centered at 130 °C. In contrast, W-KIT-6 exhibited an intense desorption peak at 125 °C, indicating more acid sites in W doped KIT-6 materials.

For W-Al-KIT-6 catalysts at Si/Al ratios of 30/1, 20/1 and 10/1, the main ammonia desorption peaks around 130–148 °C with a broad shoulder in the range of 200–500 °C range were observed, corresponding to weak and medium acid sites, respectively.[13,36] Moreover, as the aluminum content increased, the ammonia desorption peaks became more intense and the peaks shifted to higher temperature range, revealing that the total amount of acid sites and the strength of acid increased with the increasing aluminum content. Especially for W-Al-KIT-6-1, the NH_3-TPD profiles showed a drastic increase in peak intensity over 350–500 °C, indicating a drastic increase of medium acid sites under the same acid strength. The total acidity is calculated based on desorbed NH_3 from 50 to 550 °C after steady adsorption and the data are presented in Table 2. Among these materials, the total amount of acid sites increased in the following sequence: KIT-6 < W-KIT-6 < W-Al-KIT-6-30 < W-Al-KIT-6-20 < W-Al-KIT-6-10 < W-Al-KIT-6-1.

3.1.7 Raman spectroscopy. Raman spectra of various samples are shown in Fig. 7. Three peaks at 804, 716 and 272 cm^{-1} were observed for W-KIT-6 and for W-Al-KIT-6-30, which can be assigned to the symmetric stretching mode of W–O, bending mode of W–O, and deformation mode of W–O–W in the crystalline WO_3,[37,38] respectively. Compared with W-KIT-6, W-Al-KIT-6-30 showed broader Raman bands, suggesting that the dispersion of W species in W-Al-KIT-6-30 was better than that of W-KIT-6. With further increases in the aluminum content, the W-Al-KIT-6 samples showed very weak Raman peaks of crystalline WO_3, strongly suggesting that the introduction of Al could enhance the dispersion of W species in W-Al-KIT-6 (Fig. 7).

3.2. Catalytic conversion of 1-butene and ethene to propene

3.2.1 Effects of mesoporosity and Si/Al ratio. WO_3/SiO_2, W-KIT-6 and W-Al-KIT-6 catalysts are evaluated in catalytic conversion of 1-butene and ethene to propene. Possible reaction pathways are shown in Scheme 2. According to the well-established mechanism[39,40] of olefin metathesis, propene was mainly produced by the cross metathesis of 2-butene and ethene (Scheme 2a).

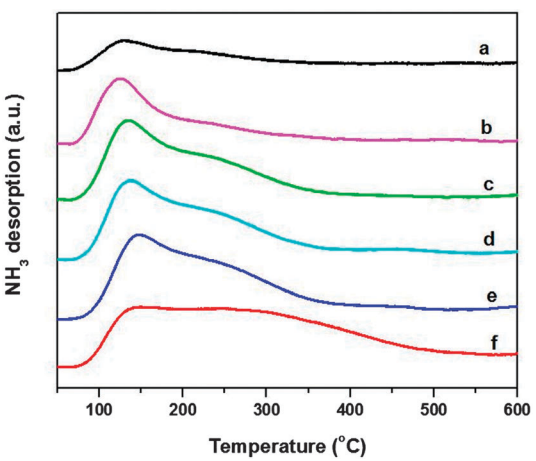

Fig. 6 NH_3-TPD profiles of different samples showing (a) KIT-6; (b) W-KIT-6; (c) W-Al-KIT-6-30; (d) W-Al-KIT-6-20; (e) W-Al-KIT-6-10; and (f) W-Al-KIT-6-1.

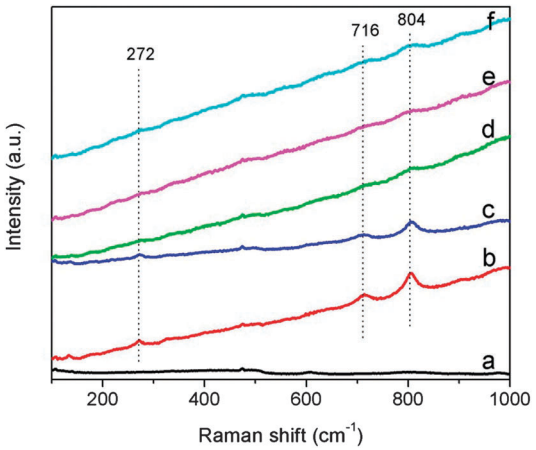

Fig. 7 Raman spectra of different samples showing (a) KIT-6; (b) W-KIT-6; (c) W-Al-KIT-6-30; (d) W-Al-KIT-6-20; (e) W-Al-KIT-6-10; and (f) W-Al-KIT-6-1.

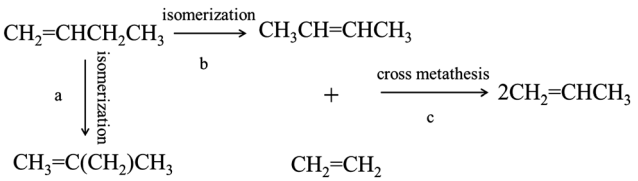

Scheme 2 The main reaction pathways of catalytic conversion of ethene and 1-butene.

Therefore, 1-butene needed to first be isomerized to 2-butene during the reaction (Scheme 2b). In our previous study,[22] MgO was used as isomerization catalysts and the catalytic reactions were conducted at 350 °C. In this study, no MgO was added, and consequently the reactions were carried out at relatively higher temperatures in the range from 400 to 500 °C.

The catalytic performances of WO_3/SiO_2, W-KIT-6 and W-Al-KIT-6 catalysts are compared in Fig. 8 and the detailed data are summarized in Table 4. WO_3/SiO_2 showed a low 1-butene conversion of 36.6% and propene selectivity of 11.0%. For mesoporous W-KIT-6, the conversion of 1-butene and selectivity of propene were 55.1% and 67.1%, respectively. As expected, these values were much better than those of conventional non-mesoporous WO_3/SiO_2 catalysts. The incorporation of a suitable amount of Al into W-KIT-6 resulted in an increase of 1-butene conversion and propene selectivity. When the Al/Si ratios increased from 1/30 to 1/10, the 1-butene conversion/propene selectivity increased from 59.5%/68.8% to 78.2%/82.4%, respectively. Moreover, at the range of Al/Si ratios from 1/30 to 1/10, the catalytic performance over W-Al-KIT-6 was quite stable. When an excess amount of Al was introduced into W-KIT-6, the 1-butene conversions and propene selectivity over W-Al-KIT-6-1 decreased, and the catalysts deactivated quickly during the first four hours of reaction.

It was suggested that highly dispersed surface tetrahedral tungsten species were active, whereas bulk WO_3 was non-active for olefin metathesis.[2] Moreover, the acidity of the support was also beneficial for olefin metathesis.[6] In the present study,

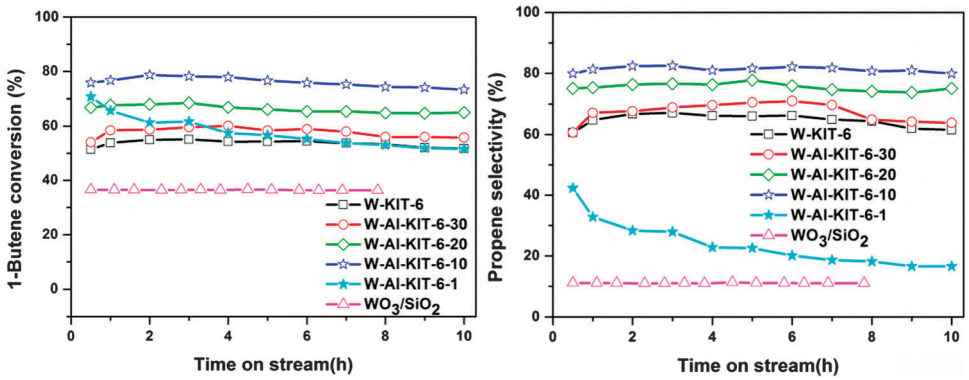

Fig. 8 1-Butene conversion (left panel) and propene selectivity (right panel) of various catalysts. Reaction conditions: catalyst weight –1.0 g; T = 450 °C; P = 0.1 MPa; WHSV = 0.8 h^{-1}; C_2H_4/1-C_4H_8 = 2.

Table 3 Effect of Si/Al ratios on conversion of 1-butene and product selectivity over W-KIT-6 and various W-Al-KIT-6 catalysts[a]

Catalysts	1-Butene conversion (%)	Selectivity (%)		
		Propene	2-Butene	Isobutene
WO_3/SiO_2	36.6	89.0	11.0	0.0
W-KIT-6	55.1	67.1	32.9	0.0
W-Al-KIT-6-30	59.5	68.8	29.4	1.8
W-Al-KIT-6-20	68.5	76.6	21.0	2.4
W-Al-KIT-6-10	78.2	82.4	12.4	5.2
W-Al-KIT-6-1	61.6	27.9	38.0	34.1

[a] Reaction conditions: catalyst weight – 1.0 g; temperature – 450 °C; pressure – 0.1 MPa; WHSV = 0.8 h^{-1}; C_2H_4/1-C_4H_8 = 2/1; data collected after 3.0 hours of reactions.

Table 4 Effect of reaction temperatures on catalytic performance over W-Al-KIT-6-10[a]

Temperature (°C)	1-Butene conversion (%)	Selectivity (%)		
		Propene	2-Butene	Isobutene
400	44.3	37.5	58.0	4.5
450	78.2	82.4	12.4	5.2
500	83.5	86.1	9.0	4.9

[a] Reaction conditions: catalyst weight – 1.0 g (W-Al-KIT-6-10); pressure – 0.1 MPa; WHSV = 0.8 h^{-1}; C_2H_4/1-C_4H_8 = 2/1.

W-KIT-6 showed a mediate catalytic performance. The doping of an appropriate amount of Al lead to an increased amount of acid sites, without changing the mesoporous structure of KIT-6 for W-Al-KIT-6 samples (Si/Al = 30/1, 20/1 and 10/1), resulting in enhanced catalytic performance. However, for W-Al-KIT-6-1 at the highest Al/Si ratio of 1/1, the collapse of mesoporous structures and an excess amount of acid sites induced by the introduction of an excess amount of Al into the framework resulted in poor catalytic performance for metathesis of 1-butene and ethene to propene. As shown in Table 3, the high acidity of W-Al-KIT-6-1 caused severe by-reactions, as evidenced by 34.1% of selectivity of isobutene. The high acidity would induce 1-butene skeletal isomerization to isobutene, as reported in the literature (Scheme 2a).[41]

It has been indicated that the amount of Al plays a crucial role in the catalytic conversion of 1-butene and ethene. At higher Si/Al ratios, W-Al-KIT-6 (Si/Al ratios of 10, 20 or 30) showed ordered mesoporous structure with moderate acidity. The moderate acidity could promote the conversion of 1-butene to 2-butene, and consequently the catalyst showed higher 1-butene conversion and propene selectivity. At low Si/Al ratios, the W-Al-KIT-6-1 catalyst exhibited high acidity and deteriorated structure. The poor texture resulted in low 1-butene conversion and the high acidity stimulated unwanted side-reaction such as, isomerization or oligomerization reactions, resulting in low propene selectivity and bad stability. W-Al-KIT-6-10 catalyst with an optimum amount of Al showed the best catalytic performance due to the highly dispersed W species and suitable acidity.

3.2.1 Effects of reaction temperature. The influence of reaction temperature on the catalytic performance of W-Al-KIT-6-10 catalysts is summarized in Table 4. At 400 °C, the catalyst showed 44.4% 1-butene conversion and 37.5% propene selectivity. When the reaction temperature increased to 450 °C, the 1-butene conversion and propene selectivity increased dramatically. Further increasing the temperature resulted in slightly improved catalytic performance.

To investigate the stability of the catalyst, a longer time on the stream reaction over W-Al-KIT-6-10 catalyst was conducted and the result is presented in Fig. S1 (ESI†). The catalyst showed slight loss of activity after 24 h of reaction. The morphology of spent catalyst was observed by TEM. The TEM image (Fig. S2, ESI†) of post-reaction W-Al-KIT-6-10 catalyst suggested that the mesoporous structure was well retained, although some domains became non-ordered. This result indicated that the catalyst showed good stability.

4. Conclusions

Ordered tungsten and aluminum co-doped mesoporous KIT-6 materials were successfully synthesized by a one-pot method, and their catalytic performances for catalytic conversion of 1-butene and ethene to propene were investigated. Characterization results revealed that the doping of an appropriate amount of Al in W-KIT-6 did not change the mesoporous structure. Moreover, the incorporation of Al could increase

the amount of acid sites and favor the dispersion of W species. When Al/Si ratios ranged from 1/30 to 1/10, W-Al-KIT-6 catalysts showed enhanced catalytic performance. The introduction of excessive Al resulted in the collapse of the mesoporous structures of KIT-6 and poor catalytic performance. The improvement of catalytic activity was ascribed to the retained mesoporous structure, the increased amount of acid sites and the better dispersion of W species facilitated by Al incorporation. The introduction of excess Al resulted in the collapse of mesoporous structure and poor catalytic performance. The findings in this study are helpful to design more efficient metathesis catalysts for propene production and could be extended to other olefin metathesis reactions.

Acknowledgements

S. Zhou thanks the financial support from the Ministry of Science and Technology of China (Grant No. 2012DFA40550) and the aided program for science and technology innovative research team of Ningbo municipality (2014B81004). K. Tao thanks the financial support from the National Natural Science Foundation of China (Grant No. 51302278) and the Natural Science Foundation of Ningbo (Grant No. 2015A610052).

References

1 J. C. Mol, *J. Mol. Catal. A: Chem.*, 2004, **213**, 39–45.
2 Q. Zhao, S.-L. Chen, J. Gao and C. Xu, *Transition Met. Chem.*, 2009, **34**, 621–627.
3 A. Spamer, T. I. Dube, D. J. Moodley, C. van Schalkwyk and J. M. Botha, *Appl. Catal., A*, 2003, **255**, 133–142.
4 N. Liu, S. Ding, Y. Cui, N. Xue, L. Peng, X. Guo and W. Ding, *Chem. Eng. Res. Des.*, 2013, **91**, 573–580.
5 M. Sibeijn and J. C. Mol, *Appl. Catal.*, 1990, **67**, 279–295.
6 S. Huang, S. Liu, W. Xin, J. Bai, S. Xie, Q. Wang and L. Xu, *J. Mol. Catal. A: Chem.*, 2005, **226**, 61–68.
7 L. Zhang, L. Shi, L. Huang, J. Zhang, R. Gao and D. Zhang, *ACS Catal.*, 2014, **4**, 1753–1763.
8 T. Xie, L. Shi, J. Zhang and D. Zhang, *Chem. Commun.*, 2014, **50**, 7250–7253.
9 H. Balcar and J. Čejka, *Coord. Chem. Rev.*, 2013, **257**, 3107–3124.
10 T. Ookoshi and M. Onaka, *Chem. Commun.*, 1998, 2399–2400.
11 L.-F. Chen, J.-C. Hu, Y.-D. Wang, K. Zhu, R. Richards, W.-M. Yang, Z.-C. Liu and W. Xu, *Mater. Lett.*, 2006, **60**, 3059–3062.
12 C. Lin, K. Tao, H. B. Yu, D. Y. Hua and S. H. Zhou, *Catal. Sci. Technol.*, 2014, **4**, 4010–4019.
13 T. I. Bhuiyan, P. Arudra, M. N. Akhtar, A. M. Aitani, R. H. Abudawoud, M. A. Al-Yami and S. S. Al-Khattaf, *Appl. Catal., A*, 2013, **467**, 224–234.
14 W. Xu, C. Lin, H. Liu, H. Yu, K. Tao and S. Zhou, *RSC Adv.*, 2015, **5**, 23981–23989.
15 X. Li, W. Zhang, S. Liu, L. Xu, X. Han and X. Bao, *J. Catal.*, 2007, **250**, 55–66.
16 D. P. Debecker, M. Stoyanova, U. Rodemerck, F. Colbeau-Justin, C. Boissere, A. Chaumonnot, A. Bonduelle and C. Sanchez, *Appl. Catal., A*, 2014, **470**, 458–466.
17 A. Tarasov, L. Kustov, V. Isaeva, A. Kalenchuk, I. Mishin, G. Kapustin and V. Bogdan, *Kinet. Catal.*, 2011, **52**, 273–276.
18 D. P. Debecker, M. Stoyanova, F. Colbeau-Justin, U. Rodemerck, C. Boissière, E. M. Gaigneaux and C. Sanchez, *Angew. Chem., Int. Ed.*, 2012, **51**, 2129–2131.
19 J. Handzlik, J. Ogonowski, J. Stoch, M. Mikołajczyk and P. Michorczyk, *Appl. Catal., A*, 2006, **312**, 213–219.
20 A. Ramanathan, B. Subramaniam, D. Badloe, U. Hanefeld and R. Maheswari, *J. Porous Mater.*, 2012, **19**, 961–968.
21 Y. H. Guo, C. Xia and B. S. Liu, *Chem. Eng. J.*, 2014, **237**, 421–429.
22 B. Hu, H. Liu, K. Tao, C. Xiong and S. Zhou, *J. Phys. Chem. C*, 2013, **117**, 26385–26395.
23 B. Hu, C. R. Xiong, K. Tao and S. H. Zhou, *J. Porous Mater.*, 2015, **22**, 613–620.
24 V. V. Balasubramanian, P. Srinivasu, C. Anand, R. R. Pal, K. Ariga, S. Velmathi, S. Alam and A. Vinu, *Microporous Mesoporous Mater.*, 2008, **114**, 303–311.
25 A. Ungureanu, B. Dragoi, V. Hulea, T. Cacciaguerra, D. Meloni, V. Solinas and E. Dumitriu, *Microporous Mesoporous Mater.*, 2012, **163**, 51–64.
26 G. Karthikeyan and A. Pandurangan, *J. Mol. Catal.*, 2012, **361–362**, 58–67.
27 A. Prabhu, L. Kumaresan, M. Palanichamy and V. Murugesan, *Appl. Catal., A*, 2009, **360**, 59–65.
28 H. Shankar, G. Rajasudha, A. Karthikeyan, V. Narayanan and A. Stephen, *Nanotechnology*, 2008, **19**, 315711.
29 F. Kleitz, F. Bérubé, R. Guillet-Nicolas, C.-M. Yang and M. Thommes, *J. Phys. Chem. C*, 2010, **114**, 9344–9355.
30 J.-C. Hu, Y.-D. Wang, L.-F. Chen, R. Richards, W.-M. Yang, Z.-C. Liu and W. Xu, *Microporous Mesoporous Mater.*, 2006, **93**, 158–163.
31 A. Ramanathan, R. Maheswari, B. P. Grady, D. S. Moore, D. H. Barich and B. Subramaniam, *Microporous Mesoporous Mater.*, 2013, **175**, 43–49.
32 S. Doniach and M. Sunjic, *J. Phys. C: Solid State Phys.*, 1970, **3**, 285.
33 X.-L. Yang, W.-L. Dai, R. Gao and K. Fan, *J. Catal.*, 2007, **249**, 278–288.
34 M. Cortés-Jácome, C. Angeles-Chavez, E. Lopez-Salinas, J. Navarrete, P. Toribio and J. Toledo, *Appl. Catal., A*, 2007, **318**, 178–189.
35 M. Occhiuzzi, D. Cordischi, D. Gazzoli, M. Valigi and P. C. Heydorn, *Appl. Catal., A*, 2004, **269**, 169–177.
36 L. Xu, C. Wang and J. Guan, *J. Solid State Chem.*, 2014, **213**, 250–255.
37 E. L. Lee and I. E. Wachs, *J. Phys. Chem. C*, 2008, **112**, 6487–6498.
38 F. Figueras, J. Palomeque, S. Loridant, C. Fèche, N. Essayem and G. Gelbard, *J. Catal.*, 2004, **226**, 25–31.
39 J. L. Herisson and Y. Chauvin, *Makromol. Chem.*, 1971, **141**, 161–167.
40 R. H. Grubbs, P. L. Burk and D. D. Carr, *J. Am. Chem. Soc.*, 1975, **97**, 3265–3267.
41 S. Meijers, L. Gielgens and V. Ponec, *J. Catal.*, 1995, **156**, 147–153.